CHAPTER 6

Numerical Simulation and Flow Visualization

6.1 Introduction

In Chapter 5, the experimental study is investigated only heat transfer performance, but the flow pattern and the related pressure drop could not be measured. In this chapter the dimple-flat tube will be investigated again. Numerical simulation of turbulent flow is employed to simulate the heat transfer performance, flow pattern and related pressure drop. In addition, smoke visualization is used to observe the flow behavior of air flow over the dimple. The results of this chapter will be compared with the previous results in Chapter 5.

6.2 Numerical simulation of flat-dimple tube

6.2.1 Problem conditions and main assumptions

Figure 6.1 shows the simulated dimple-flat tube. The simulated conditions are set up to be the same as the previous experiment. The problem under consideration is air flow across the single tube with constant temperature at the surface. The problem has the following conditions:

- The inlet fluid is air at 300 K.
- The entrance air velocity is varied from 1 to 3 m/s.
- The constant surface temperature of 400 K is applied to the surface of the flat-dimple tube.
- The boundary conditions are the no-slip conditions at the surface
- No conduction heat transfer in the solid.
- The air flow is assumed to be steady state in a three-dimensional domain.

ลิขสิทธิ์มหาวิทยาลัยเชียงใหม่
Copyright© by Chiang Mai University
All rights reserved

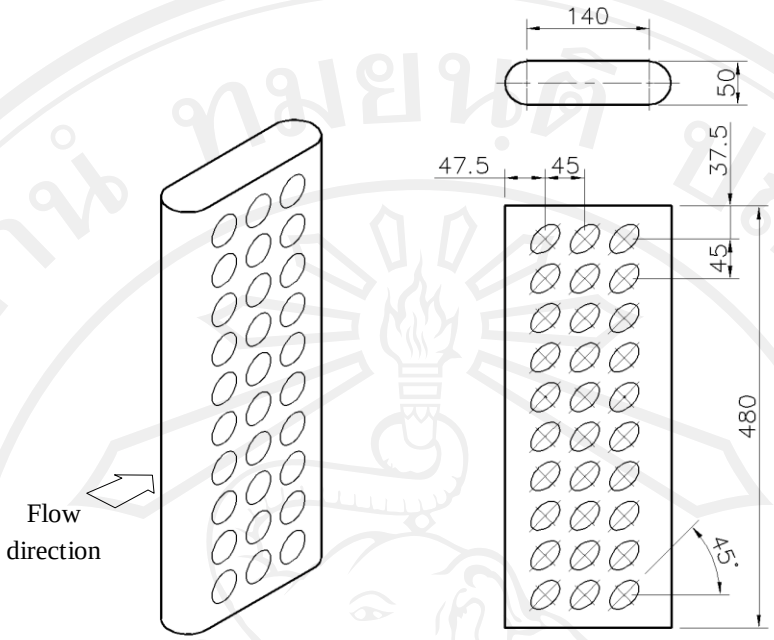

Figure 6.1 Details of a flat-dimple tube (all dimensions are in mm).

6.2.2 Numerical method

The numerical solutions of turbulent flow are obtained by using the SOLIDWORKS Flow Simulation 2012. The k-ε model is employed as the turbulence model for all numerical predictions similar to Chapter 2. The governing equations for the present system can be expressed and obtained as shown in Chapter 2

Figure 6.2 shows a side view of the computational grid of a flat-dimple tube. The computational domain size is shown in Table 6.1. From a grid independent test, it was found that the basic mesh dimensions and numbers of cells are shown in Table 6.2.

ลิขสิทธิ์มหาวิทยาลัยเชียงใหม่
Copyright© by Chiang Mai University
All rights reserved

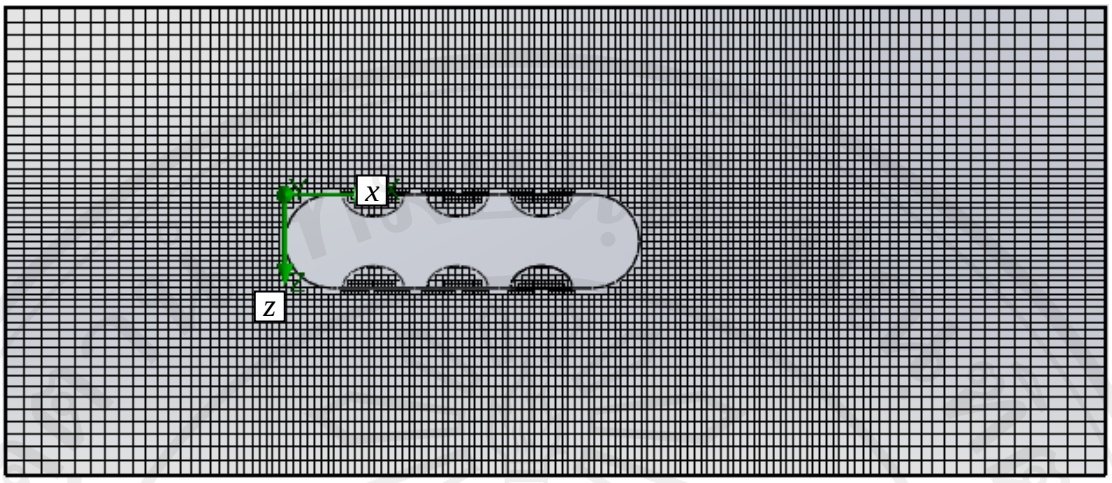

Figure 6.2 Computational grids for a flat-dimple tube.

Table 6.1 Computational domain size.

Dimension	Flat-dimple tube
X min	-150.0 mm
X max	440.0 mm
Y min	-480.0 mm
Y max	0 mm
Z min	-100.0 mm
Z max	150.0 mm

Table 6.2 Basic mesh dimensions and numbers of cell.

Detail	Flat-dimple tube
Number of cells in X	129
Number of cells in Y	136
Number of cells in Z	52
Total cells	920,898
Fluid cells	813,635
Solid cells	80,275
Partial cells	26,988

ลิขสิทธิ์มหาวิทยาลัยเชียงใหม่
Copyright© by Chiang Mai University
All rights reserved

6.2.3 Data reduction

The air side heat transfer rate and the total force in the stream line direction are obtained to determine the heat transfer coefficient and the drag coefficient. The averaged air side heat transfer coefficient (h) is calculated by

$$h = q_s'' / (T_s - T_\infty) \tag{6.1}$$

where q'' is the surface heat flux. The heat flux is calculated from heat rate level at the tested surface divided by the surface area. The surface area does not include the dimple surface (flat portion only). T_s is surface temperature and T_∞ is temperature of inlet air stream flowing over the tube.

The drag coefficient is calculated by

$$C_d = \frac{F_x}{\rho V_f^2 A_f / 2} \tag{6.2}$$

where F_x is total force in x-direction. ρ_f and V_f are the density of the air and the air frontal velocity respectively. For a cylinder, A_f = (P/π)×L_t where P is the perimeter of the flat tube and L_t is the tube length. For a flat-dimple tube, A_f = D×L_t by D is the tube width.

6.2.4 Results and discussions

In this part, the numerical simulation of air flow across the flat–dimple tube was investigated. In addition, air flow across a round tube was investigated to compare with a flat–dimple tube. Figure 6.3 shows the average air side heat transfer coefficient of a flat-dimple tube by experimental and numerical simulation, and the heat transfer coefficient of cylinder by numerical simulation and the model from Hilpert (1933). As shown in the figure, both results have the trend. Although the numerical result of the flat-dimple tube has an error of about 9% from the experimental result. Similar to the results of the cylinder, the numerical result has an error of about 8% from the model of Hilpert (1933) and both results have the same trend.

ลิขสิทธิ์มหาวิทยาลัยเชียงใหม่
Copyright© by Chiang Mai University
All rights reserved

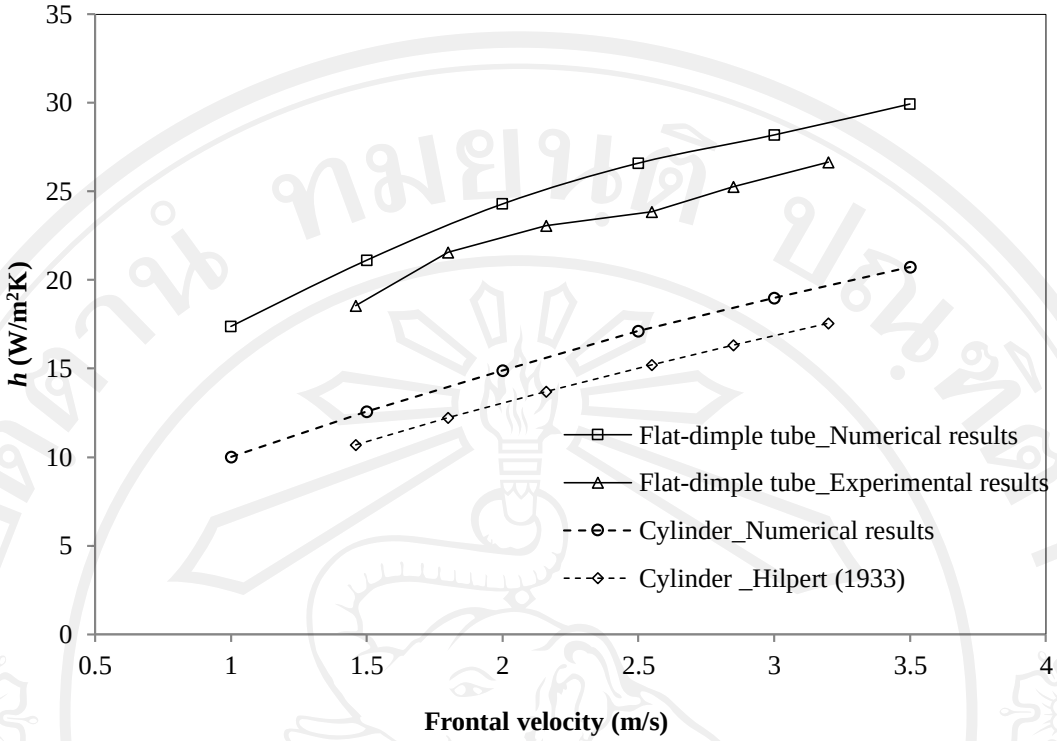

Figure 6.3 Comparison of average heat transfer coefficient of experimental results and numerical results of flat-dimple tube and cylinder**.**

Figure 6.4 shows the drag coefficient of a flat-dimple tube from numerical simulations, and the drag coefficient of a cylinder from numerical simulation and the model of Schlichting (2000). As shown in the figure, the numerical results and the model have similar trends of values of the drag coefficient. The error is about 25%. At a frontal velocity of 1.2 m/s, flow separation appears at the top and bottom of the cylinder. At these points the velocity is a maximum. This phenomenon establishes low pressure at the wake region; thus the pressure difference and drag coefficient increases. For a flat-dimple tube, the drag coefficient slightly decreases as the frontal velocity increases; this result is different from the cylinder because at a frontal velocity of 1-4 m/s, the separation points don't move to the top and the bottom of the tube, thus the drag coefficient increase as the frontal velocity increase. In addition, the drag coefficient of a flat-dimple tube has lower values than the numerical results by about 25-30%.

ลิขสิทธิ์มหาวิทยาลัยเชียงใหม่
Copyright© by Chiang Mai University
All rights reserved

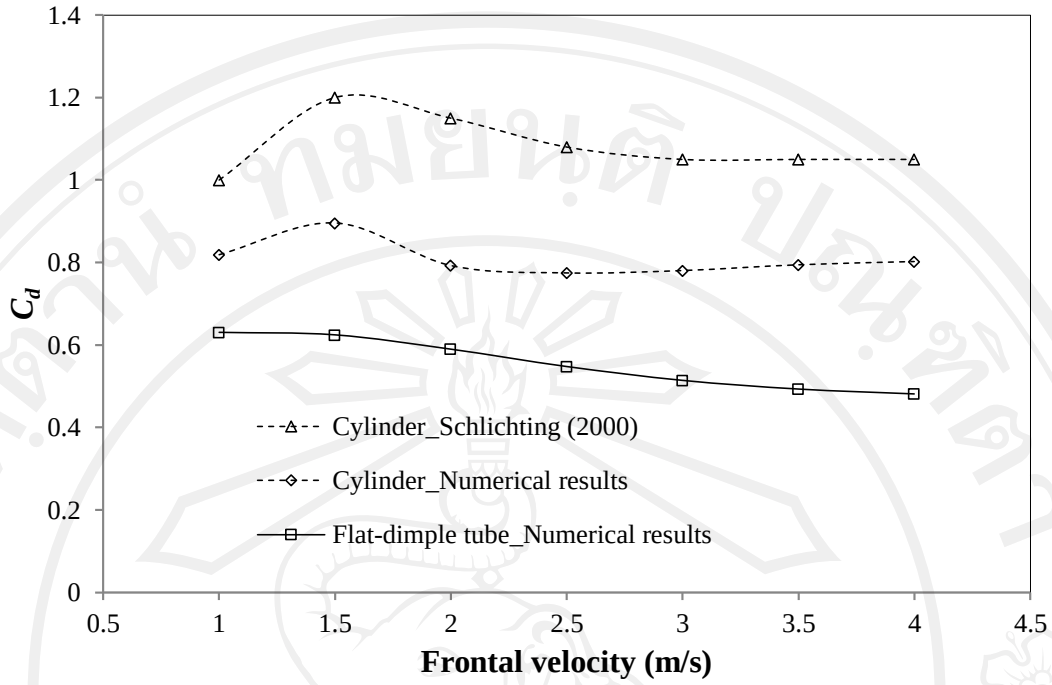

Figure 6.4 Drag coefficients of flat-dimple tube and cylinder in comparison of numerical results and the model.

6.3 Flow visualization and flow structure

6.3.1 Smoke visualization

Figure 6.5 shows flow visualization of air flow over the dimple surfaces. Flow visualization using smoke is used to observe the flow structures. As shown in the figure, as the smoke is advected downstream, the recirculation flow occurs inside the dimple and flow dispersion is developed after smoke attacks the downstream rim of dimple. The recirculation and dispersion is established only at the lower streamline, while the upper streamlines crossover the dimple.

ลิขสิทธิ์มหาวิทยาลัยเชียงใหม่
Copyright© by Chiang Mai University
All rights reserved

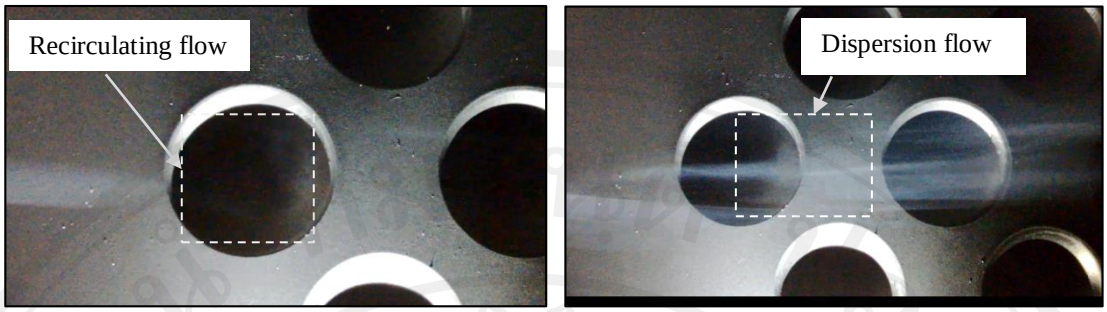

(a)

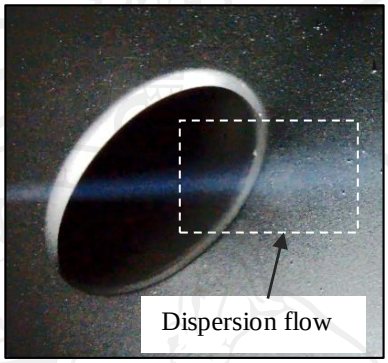

(b)

Figure 6.5 Flow visualization of: (a) spherical dimpled surface, and (b) ellipsoidal dimpled surface.

6.3.2 Effect of flow structure on temperature distribution

The temperature distribution along the stream line of a spherical dimple surface (Geometric No.1 in Chapter 3) is illustrated in Figure 6.6. As shown in the figure, variations with y are given along a line corresponding to x = 20 mm. The bulk flow stream direction is from the left hand side. It is found that higher temperatures are located over the upstream halves of the dimple. Local temperatures are then lower in the downstream halves. The lowest values are located near the downstream rim of the dimple. The regions of low temperatures are the result of the dispersion flow that is established at the downstream rim of the dimple. The effects of this phenomenon on thermal transport are especially pronounced near the downstream rim of the dimple as well as on the flat surface downstream of the dimple and in between the dimples. This phenomenon

ลิขสิทธิ์มหาวิทยาลัยเชียงใหม่
Copyright© by Chiang Mai University
All rights reserved

produces heat transfer augmentation from the unsteadiness of the dispersion fluid near the surface.

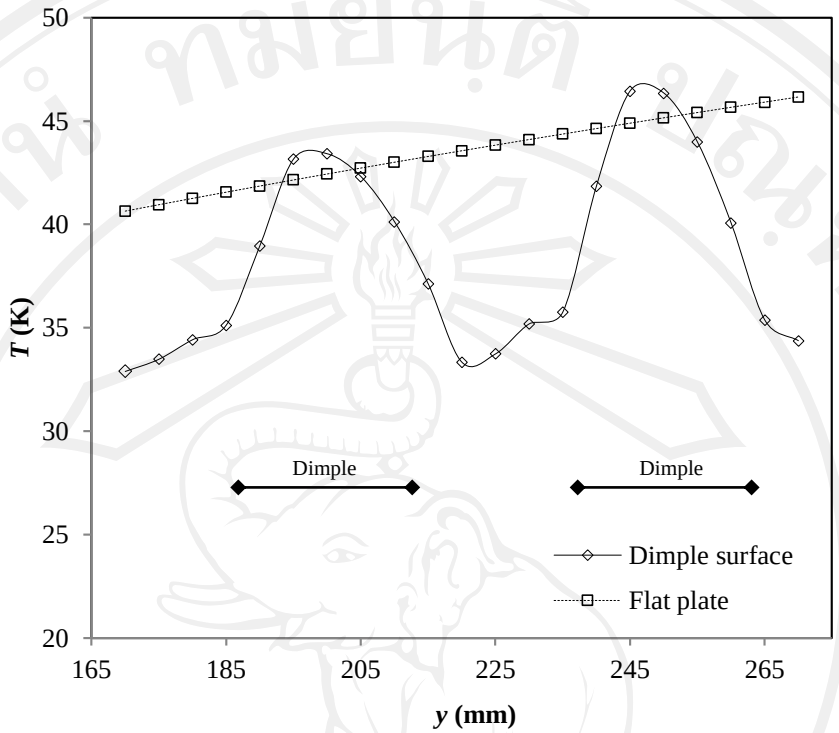

Figure 6.6 Temperature distribution along the stream line of spherical dimple surface of Geometric No.1 at frontal velocity 4.1 m/s.

6.4 Summary and conclusion

The present study reports the heat transfer performance, drag coefficient, and flow behavior of air over a flat-dimple tube. The results of this work are compared with experimental results from the previous chapters. On the basis of previous discussions, the following conclusions are made:

1) From the numerical results, flat-dimple tube has a lower drag coefficient than the cylinder by about 30%.

2) Recirculation flow occurs inside the dimple and flow dispersion is developed after smoke exits the downstream rim of the dimple. The dispersion flow produces heat transfer augmentation from the unsteadiness of the flow near the surface.

ลิขสิทธิ์มหาวิทยาลัยเชียงใหม่
Copyright© by Chiang Mai University
All rights reserved